Iranian Journal of Mathematical chemistry

IJMC

DOI: 10.22052/ijmc.2026.258327.2112
Vol. 17, No. 4, 2026, pp. 415-437
Research Paper

An Innovative Numerical Approach for Solving Two-Dimensional Helmholtz Problem

Soheila Heidari [1] and Mahmoud Behroozifar [1*]

[1]Department of Mathematics, Babol Noshirvani University of Technology, Babol, Iran

Keywords:
Helmholtz problem,
Homogenizing Gegenbauer polynomials,
Generalized interpolation,
Spectral method,
Non-homogeneous boundary conditions

AMS Subject Classification (2020):
65N30; 65N35; 35J05; 33C45

Article History:
Received: 2 February 2026
Accepted: 14 July 2026

Abstract

This paper proposes a new spectral approach for the two-dimensional Helmholtz equation with Dirichlet boundary conditions. We construct a closed-form two-dimensional generalized interpolation function that exactly satisfies arbitrary (non-homogeneous) boundary data, reducing the original problem to an equivalent one with homogeneous boundary conditions. To approximate the homogenized problem, we introduce a two-variable family of homogenizing Gegenbauer polynomials (HGPs) that vanish identically on the domain boundary, and show that the resulting basis is semi-orthogonal with a banded (pentadiagonal) Gram matrix, preserving the computational efficiency of spectral methods. A Galerkin discretization then reduces the problem to a system of algebraic equations. We derive an explicit upper bound on the approximation error and prove a spectral (exponential) convergence rate for analytic solutions. Eight benchmark problems - including Helmholtz and Poisson equations with separable and non-separable exact solutions, constant and variable coefficients, and a classical torsion-problem benchmark - are used to assess accuracy, stability under boundary and source-term perturbations, and CPU efficiency. The proposed method achieves low RMSE values with low polynomial degree ($M \leq 4$) and modest CPU time, and compares favorably with existing finite element, finite difference, and spectral element approaches reported in the literature.

© 2026 University of Kashan Press. All rights reserved

*Corresponding author
E-mail addresses: m97heidari.s@gmail.com (S. Heidari), m_behroozifar@nit.ac.ir, behroozifar2@gmail.com (M. Behroozifar)
Academic Editor: Yadollah Ordokhani

1 Introduction

The Helmholtz equation, named after Hermann von Helmholtz, is a fundamental partial differential equation arising in both physics and applied mathematics. It plays a central role in modeling a wide range of physical phenomena, including time-harmonic acoustic and electromagnetic fields [1–6], acoustic wave scattering [7–9], quantum mechanics [10], water wave propagation, membrane vibrations [11, 12], radar scattering [13, 14], fluid dynamics [15], and optics [16, 17]. Consequently, the development of efficient and accurate numerical methods for solving the Helmholtz and related Poisson equations has attracted considerable research attention.

In [18], time-harmonic scattering problems are addressed using a high-order Nyström discretization of boundary integral equations in both two and three dimensions. A key feature of this approach is the incorporation of local corrections near kernel singularities. The study in [19] investigates pollution effects and evaluates the performance of the discrete singular convolution (DSC) method for high-wavenumber Helmholtz problems, with Fourier analysis employed to assess dispersive errors. In [20], a compact high-order finite difference scheme is combined with a multigrid V-cycle algorithm for solving the two-dimensional Poisson equation with Dirichlet boundary conditions. A neural network-based framework for solving the two-dimensional Helmholtz equation is presented in [21], where constrained optimization problems are reformulated into unconstrained ones via Lagrange multiplier and trial function methods. Furthermore, conditioning issues associated with Helmholtz discretizations are examined in [22], highlighting that, although large wave numbers often lead to ill-conditioned systems, certain discretizations exhibit improved conditioning behavior. According to [23], the Galerkin method can outperform classical finite element methods in terms of memory usage and computational efficiency for solving the two-dimensional Helmholtz equation.

The present paper considers the following two-dimensional Helmholtz equation [24, 25]:

$$\nabla^2 u + f(x,y)u = g(x,y), \quad (x,y) \in [a,b] \times [c,d], \tag{1}$$

subject to the Dirichlet boundary conditions

$$u(a,y) = f_1(y), \quad u(b,y) = f_2(y), \quad c \le y \le d, \tag{2}$$

$$u(x,c) = f_3(x), \quad u(x,d) = f_4(x), \quad a \le x \le b. \tag{3}$$

Here, $\nabla^2 u = u_{xx} + u_{yy}$ denotes the two-dimensional Laplace operator, and $u(x,y)$ is the unknown function. Equation (1) reduces to the classical oscillatory Helmholtz equation when $f(x,y) = k = \lambda^2 > 0$, where λ is the wave number. If $f(x,y) = 0$, it becomes the Poisson equation, whereas for $f(x,y) = k < 0$, it corresponds to the monotone Helmholtz equation. The Helmholtz equation admits various fundamental solutions depending on the spatial domain and physical context [26].

The two-dimensional Helmholtz equation also plays an important role in chemistry. In particular, it arises in computational quantum chemistry through its connection with the time-independent Schrödinger equation for confined systems such as quantum dots [27, 28]. It is further used in modeling optical fields in spectroscopy, including evanescent wave sensors and laser cavity modes [17]. Additional applications include diffusion–reaction systems, electrochemical processes, and spectroscopic techniques such as infrared and Raman spectroscopy, where it describes resonance phenomena and energy localization [17].

The novelty of the present work is threefold.

- First, we derive a closed-form two-dimensional generalized interpolation function capable of exactly matching arbitrary non-homogeneous boundary data on a rectangular domain,

together with explicit compatibility conditions guaranteeing its existence. We construct an interpolation function $w(x, y)$ that exactly satisfies the prescribed boundary conditions,

$$\begin{aligned} w(a, y) &= u(a, y), \quad w(b, y) = u(b, y), \quad c \leq y \leq d, \\ w(x, c) &= u(x, c), \quad w(x, d) = u(x, d), \quad a \leq x \leq b, \end{aligned}$$

thereby enabling a transformation of the original Helmholtz problem into an equivalent problem with homogeneous boundary conditions.

- Second, we construct a new class of two-variable homogenizing Gegenbauer polynomials that vanish identically on the domain boundary by design, and we prove that this basis is semi-orthogonal with a pentadiagonal Gram matrix - a property that, to the best of our knowledge, has not been established for boundary-vanishing Gegenbauer-type bases in two dimensions. We further show that this sparsification preserves the spectral (exponential) convergence rate characteristic of fully orthogonal expansions, so boundary-condition enforcement is achieved without sacrificing computational efficiency or approximation accuracy.

- Third, we derive an explicit upper bound for the resulting approximation error and establish a rigorous convergence theory covering both finitely smooth and analytic solutions. The combined framework is validated on a range of benchmark Helmholtz and Poisson problems - including cases with variable coefficients and non-separable exact solutions - and is shown to attain high accuracy at low polynomial degree and modest computational cost, compared favorably with existing finite element, finite difference, and spectral element approaches reported in the literature.

The remainder of this paper is organized as follows. Subsection 2.1 introduces the proposed interpolation technique. Subsection 2.2 reviews Gegenbauer polynomials and presents the construction of homogenizing Gegenbauer polynomials. Subsection 2.3 investigates the inner product properties of the shifted expansion functions. Subsection 2.4 describes the approximation strategy. Section 3 is devoted to the derivation of the upper bound of the approximation error and the analysis of the convergence properties of the proposed approximation. Section 4 details the method for solving the Helmholtz problem. Numerical results are presented in Section 5, and concluding remarks are given in the final section.

2 Preliminary topics

2.1 Interpolation function

In this subsection, we construct a function $w(x, y)$ that satisfies the boundary conditions given in Equations (2) and (3). Specifically, we seek a function $w(x, y)$ such that

$$w(a, y) = f_1(y), \quad w(b, y) = f_2(y), \quad w(x, c) = f_3(x), \quad w(x, d) = f_4(x). \tag{4}$$

To ensure the existence of such a function, the following compatibility conditions must hold:

$$\begin{aligned} f_1(c) &= w(a, c) = f_3(a), \quad f_2(d) = w(b, d) = f_4(b), \\ f_2(c) &= w(b, c) = f_3(b), \quad f_1(d) = w(a, d) = f_4(a). \end{aligned} \tag{5}$$

If these conditions are not satisfied, the problem defined by (4) does not admit a solution.

To construct $w(x,y)$, we consider the following ansatz:

$$w(x,y) = A_0(y) + A_1(y)(x-a) + A_2(x)(x-a)(x-b) + A_3(x)(x-a)(x-b)(y-c), \tag{6}$$

where the coefficient functions $A_0(y), A_1(y), A_2(x), A_3(x)$ are determined by enforcing the boundary conditions:

$$w(a,y) = f_1(y), \quad w(b,y) = f_2(y), \quad w(x,c) = f_3(x), \quad w(x,d) = f_4(x). \tag{7}$$

Solving the system (7) yields

$$A_0(y) = f_1(y), \quad A_1(y) = -\frac{f_2(y) - f_1(y)}{a-b}, \tag{8}$$

$$A_2(x) = -\frac{aA_1(c) - xA_1(c) - A_0(c) + f_3(x)}{(a-x)(x-b)},$$

$$A_3(x) = -\frac{aA_1(c) - aA_1(d) - xA_1(c) - A_0(c) + xA_1(d) + A_0(d) + f_3(x) - f_4(x)}{(a-x)(x-b)(c-d)}. \tag{9}$$

By substituting (8) and (9) into (6), and using the compatibility conditions (5), we obtain:

$$\begin{aligned} w(x,y) &= \frac{1}{(a-b)(c-d)}\Big[f_4(a)(b-x)(c-y) - f_4(b)(a-x)(c-y) - f_3(a)(b-x)(d-y) \\ &+ f_3(b)(a-x)(d-y) + (a-x)(c-d)f_2(y) \\ &- (b-x)(c-d)f_1(y) + acf_4(x) - adf_3(x) + ayf_3(x) - ayf_4(x) \\ &- bcf_4(x) + bdf_3(x) - byf_3(x) + byf_4(x)\Big]. \end{aligned} \tag{10}$$

The function defined in (10) is referred to as the *two-dimensional generalized interpolating function*. It can be verified directly that, under the compatibility conditions (5), this function satisfies all boundary conditions specified in (4).

2.2 Homogenizing Gegenbauer polynomials

Gegenbauer polynomials, also referred to as ultraspherical polynomials and denoted by $C_n^{(\lambda)}(r)$, are the solutions of the Gegenbauer differential equation for non-negative integers n:

$$(1-r^2)y'' - (2\lambda+1)ry' + n(n+2\lambda)y = 0.$$

These polynomials form an orthogonal system on the interval $[-1,1]$ with respect to the weight function $(1-r^2)^{\lambda-\frac{1}{2}}$ [29–31]. For particular values of λ, they reduce to well-known families: Legendre polynomials ($\lambda = \frac{1}{2}$), Chebyshev polynomials of the first kind ($\lambda = 0$), and Chebyshev polynomials of the second kind ($\lambda = 1$).

Gegenbauer polynomials are a special case of Jacobi polynomials $J_n^{(\alpha,\beta)}(r)$, obtained by setting $\alpha = \beta = \lambda - \frac{1}{2}$:

$$C_n^{(\lambda)}(r) = \frac{\Gamma\left(\lambda+\frac{1}{2}\right)}{\Gamma(2\lambda)} \frac{\Gamma(n+2\lambda)}{\Gamma\left(n+\lambda+\frac{1}{2}\right)} J_n^{\left(\lambda-\frac{1}{2},\lambda-\frac{1}{2}\right)}(r),$$

see [29, 32]. They satisfy the three-term recurrence relation

$$nC_n^{(\lambda)}(r) = 2r(n+\lambda-1)C_{n-1}^{(\lambda)}(r) - (n+2\lambda-2)C_{n-2}^{(\lambda)}(r),$$

with initial conditions

$$C_0^{(\lambda)}(r) = 1, \qquad C_1^{(\lambda)}(r) = 2\lambda r,$$

and admit the generating function

$$\frac{1}{(1-2rt+t^2)^{\lambda}} = \sum_{n=0}^{\infty} C_n^{(\lambda)}(r)t^n,$$

see [30, 31]. The first few Gegenbauer polynomials are given by:

$$\begin{aligned} C_0^{(\lambda)}(r) &= 1, \qquad C_1^{(\lambda)}(r) = 2\lambda r, \\ C_2^{(\lambda)}(r) &= -\lambda + 2\lambda(1+\lambda)r^2, \\ C_3^{(\lambda)}(r) &= -2\lambda(1+\lambda)r + \frac{4}{3}\lambda(1+\lambda)(2+\lambda)r^3. \end{aligned}$$

In this subsection, our objective is to construct *homogenizing Gegenbauer polynomials* that vanish on the boundary of the rectangular domain $[a,b]\times[c,d]$. Such basis functions are particularly useful in spectral methods for incorporating homogeneous boundary conditions [31, 32].

We first define the function

$$H_1(k,x) = \alpha C_{k+1}^{(\lambda)}\left(\frac{-a-b+2x}{b-a}\right) + \beta C_k^{(\lambda)}\left(\frac{-a-b+2x}{b-a}\right) + C_{k+2}^{(\lambda)}\left(\frac{-a-b+2x}{b-a}\right), \tag{11}$$

where $C_k^{(\lambda)}\left(\frac{-a-b+2x}{b-a}\right)$ denotes the shifted Gegenbauer polynomial on $[a,b]$, and α, β are parameters to be determined. Imposing the boundary conditions

$$H_1(k,a) = 0, \quad H_1(k,b) = 0,$$

leads to a linear system for α and β, yielding

$$\alpha = -\frac{C_{k+2}^{(\lambda)}(1)C_k^{(\lambda)}\left(\frac{a-b}{b-a}\right) - C_k^{(\lambda)}(1)C_{k+2}^{(\lambda)}\left(\frac{a-b}{b-a}\right)}{C_{k+1}^{(\lambda)}(1)C_k^{(\lambda)}\left(\frac{a-b}{b-a}\right) - C_k^{(\lambda)}(1)C_{k+1}^{(\lambda)}\left(\frac{a-b}{b-a}\right)}, \tag{12}$$

$$\beta = -\frac{C_{k+2}^{(\lambda)}(1)C_{k+1}^{(\lambda)}\left(\frac{a-b}{b-a}\right) - C_{k+1}^{(\lambda)}(1)C_{k+2}^{(\lambda)}\left(\frac{a-b}{b-a}\right)}{C_k^{(\lambda)}(1)C_{k+1}^{(\lambda)}\left(\frac{a-b}{b-a}\right) - C_{k+1}^{(\lambda)}(1)C_k^{(\lambda)}\left(\frac{a-b}{b-a}\right)}.$$

Substituting these expressions into (11), we obtain:

$$\begin{aligned} H_1(k,x) &= C_{k+2}^{(\lambda)}\left(\frac{-a-b+2x}{b-a}\right) + \\ &\frac{-\left(C_{k+2}^{(\lambda)}(1)C_{k+1}^{(\lambda)}\left(\frac{a-b}{b-a}\right) - C_{k+1}^{(\lambda)}(1)C_{k+2}^{(\lambda)}\left(\frac{a-b}{b-a}\right)\right)C_k^{(\lambda)}\left(\frac{-a-b+2x}{b-a}\right)}{C_k^{(\lambda)}(1)C_{k+1}^{(\lambda)}\left(\frac{a-b}{b-a}\right) - C_{k+1}^{(\lambda)}(1)C_k^{(\lambda)}\left(\frac{a-b}{b-a}\right)} + \\ &\frac{-\left(C_{k+2}^{(\lambda)}(1)C_k^{(\lambda)}\left(\frac{a-b}{b-a}\right) - C_k^{(\lambda)}(1)C_{k+2}^{(\lambda)}\left(\frac{a-b}{b-a}\right)\right)C_{k+1}^{(\lambda)}\left(\frac{-a-b+2x}{b-a}\right)}{C_{k+1}^{(\lambda)}(1)C_k^{(\lambda)}\left(\frac{a-b}{b-a}\right) - C_k^{(\lambda)}(1)C_{k+1}^{(\lambda)}\left(\frac{a-b}{b-a}\right)}, \end{aligned} \tag{13}$$

which defines the homogenizing Gegenbauer polynomials on $[a, b]$ satisfying

$$H_1(k, a) = 0, \quad H_1(k, b) = 0.$$

By an analogous construction, we define $H_2(k, y)$ on $[c, d]$ such that

$$H_2(k, c) = 0, \quad H_2(k, d) = 0,$$

leading to

$$\begin{aligned} H_2(k,y) &= C_{k+2}^{(\lambda)}\left(\frac{-c-d+2y}{d-c}\right) + \\ &\frac{-\left(C_{k+2}^{(\lambda)}(1)C_{k+1}^{(\lambda)}\left(\frac{c-d}{d-c}\right) - C_{k+1}^{(\lambda)}(1)C_{k+2}^{(\lambda)}\left(\frac{c-d}{d-c}\right)\right)C_k^{(\lambda)}\left(\frac{-c-d+2y}{d-c}\right)}{C_k^{(\lambda)}(1)C_{k+1}^{(\lambda)}\left(\frac{c-d}{d-c}\right) - C_{k+1}^{(\lambda)}(1)C_k^{(\lambda)}\left(\frac{c-d}{d-c}\right)} + \\ &\frac{-\left(C_{k+2}^{(\lambda)}(1)C_k^{(\lambda)}\left(\frac{c-d}{d-c}\right) - C_k^{(\lambda)}(1)C_{k+2}^{(\lambda)}\left(\frac{c-d}{d-c}\right)\right)C_{k+1}^{(\lambda)}\left(\frac{-c-d+2y}{d-c}\right)}{C_{k+1}^{(\lambda)}(1)C_k^{(\lambda)}\left(\frac{c-d}{d-c}\right) - C_k^{(\lambda)}(1)C_{k+1}^{(\lambda)}\left(\frac{c-d}{d-c}\right)}. \end{aligned} \tag{14}$$

These homogenizing Gegenbauer polynomials provide a convenient basis for constructing two-dimensional approximation spaces that inherently satisfy homogeneous boundary conditions, thereby simplifying the numerical treatment of boundary value problems. The constructed functions $H_1(k, x)$ and $H_2(k, y)$ form boundary-vanishing basis functions, which can be directly employed in spectral approximations of elliptic problems with homogeneous Dirichlet boundary conditions.

2.3 Inner product properties of the shifted expansion functions

To facilitate the spectral discretization of the governing equations, we investigate the orthogonality and inner product properties of the linear combination of Gegenbauer polynomials. Let the expansion functions $H_1(k, x)$ be defined on the domain $[0, L_1]$ as:

$$H_1(k, x) = C_{k+2}^{\lambda}(\xi(x)) + \alpha C_{k+1}^{\lambda}(\xi(x)) + \beta C_k^{\lambda}(\xi(x)),$$

where $\xi(x) = \frac{2}{L_1}x - 1$ maps the interval $x \in [0, L_1]$ onto the standard domain $\xi \in [-1, 1]$. The associated shifted weight function is defined as:

$$w_{L_1}(x) = \left[1 - \left(\frac{2}{L_1}x - 1\right)^2\right]^{\lambda - \frac{1}{2}}.$$

By utilizing the standard orthogonality relation of the classical Gegenbauer polynomials:

$$\int_{-1}^{1} C_n^{\lambda}(\xi) C_m^{\lambda}(\xi)(1 - \xi^2)^{\lambda - \frac{1}{2}}\, d\xi = \delta_{nm} h_n^{\lambda},$$

where δ_{nm} denotes the Kronecker delta, and h_n^{λ} represents the normalization factor given by:

$$h_n^{\lambda} = \frac{\pi 2^{1-2\lambda}\Gamma(n + 2\lambda)}{n!(n + \lambda)[\Gamma(\lambda)]^2}.$$

The inner product integrals $I_m = \int_0^{L_1} H_1(k, x) H_1(k + m, x) w_{L_1}(x)\, dx$ for $m = 0, 1, 2$ can be evaluated analytically. Due to the orthogonality of terms with non-matching degrees, the cross-multiplications vanish, leaving the following exact closed-form expressions:

1. Diagonal terms ($m = 0$)

$$\int_0^{L_1} [H_1(k,x)]^2 w_{L_1}(x)\,dx = \frac{L_1}{2}\left(h^\lambda_{k+2} + \alpha^2 h^\lambda_{k+1} + \beta^2 h^\lambda_k\right).$$

2. First superdiagonal terms ($m = 1$)

$$\int_0^{L_1} H_1(k,x)H_1(k+1,x)w_{L_1}(x)\,dx = \frac{L_1}{2}\left(\alpha h^\lambda_{k+2} + \alpha\beta h^\lambda_{k+1}\right).$$

3. Second superdiagonal terms ($m = 2$)

$$\int_0^{L_1} H_1(k,x)H_1(k+2,x)w_{L_1}(x)\,dx = \frac{L_1}{2}\left(\beta h^\lambda_{k+2}\right).$$

For all higher shifts where $m \geq 3$, the expansion functions share no overlapping polynomial degrees, yielding:

$$\int_0^{L_1} H_1(k,x)H_1(k+m,x)w_{L_1}(x)\,dx = 0, \quad \forall m \geq 3.$$

Substituting the explicit representation of h^λ_n into the equations above yields the final computational formulas:

$$\int_0^{L_1} [H_1(k,x)]^2 w_{L_1}(x)\,dx = \Lambda\left[\frac{\Gamma(k+2\lambda+2)}{(k+2)!(k+\lambda+2)} + \alpha^2\frac{\Gamma(k+2\lambda+1)}{(k+1)!(k+\lambda+1)} + \beta^2\frac{\Gamma(k+2\lambda)}{k!(k+\lambda)}\right],$$

$$\int_0^{L_1} H_1(k,x)H_1(k+1,x)w_{L_1}(x)\,dx = \Lambda\left[\alpha\frac{\Gamma(k+2\lambda+2)}{(k+2)!(k+\lambda+2)} + \alpha\beta\frac{\Gamma(k+2\lambda+1)}{(k+1)!(k+\lambda+1)}\right],$$

$$\int_0^{L_1} H_1(k,x)H_1(k+2,x)w_{L_1}(x)\,dx = \Lambda\left[\beta\frac{\Gamma(k+2\lambda+2)}{(k+2)!(k+\lambda+2)}\right],$$

where, the common scaling factor Λ is defined as:

$$\Lambda = \frac{L_1\pi 2^{-2\lambda}}{[\Gamma(\lambda)]^2}.$$

The algebraic properties established above demonstrate that the sequence of functions $\{H_1(k,x)\}_{k=0}^N$ constitutes a **semi-orthogonal basis** with respect to the weighted inner product space $L^2_w([0,L_1])$. The associated Gram matrix

$$\int_0^{L_1} \phi_1(x)\,\phi_1(x)^T\,dx,$$

is banded, specifically, at most pentadiagonal, rather than fully populated, regardless of the basis dimension.

While a strictly orthogonal basis yields a purely diagonal representation, such bases frequently lack the capacity to satisfy prescribed boundary conditions implicitly. By defining $H_1(k,x)$ as a compact linear combination of three consecutive Gegenbauer polynomials, the basis functions can be constructed to satisfy the underlying physical boundary conditions of the differential equation while strictly limiting the spread of non-zero inner products. Because

$\langle H_1(i,x), H_1(j,x)\rangle_w = 0$ for all $|i-j| > 2$, the semi-orthogonality ensures that the resulting system matrices retain a tightly bounded, pentadiagonal structure. This framework successfully bridges the gap between boundary condition enforcement and optimal computational efficiency.

Because a banded matrix of this type is sparse rather than dense, additional preconditioning or stabilization is unnecessary to maintain numerical stability. Furthermore, transitioning from a purely orthogonal to a semi-orthogonal basis does not alter the underlying approximation space; it merely changes the coordinate system within it. Consequently, for smooth solutions, the expansion coefficients continue to exhibit exponential (or sub-exponential) decay, thereby preserving the classical spectral accuracy of the method.

2.4 Function approximation

Let $G = L^2[a_0, b_0]$ be a Hilbert space and let $\{x_0(t), x_1(t), \ldots, x_m(t)\} \subset G$ be a linearly independent set. Define the finite-dimensional subspace

$$Y = \text{Span}\{x_0(t), x_1(t), \ldots, x_m(t)\}.$$

For an arbitrary element $f^* \in G$, there exists a unique best approximation $y_0 \in Y$ such that [33]

$$\|f^* - y_0\|_2 \leq \|f^* - y\|_2, \quad \forall y \in Y,$$

where $\|f\|_2 = \sqrt{\langle f, f\rangle}$ and $\langle f, g\rangle = \int_{a_0}^{b_0} f(t)g(t)\,dt$ denotes the inner product in G.

Hence, f^* admits the representation

$$f^*(t) \approx y_0(t) = \sum_{i=0}^{m} c_i x_i(t) = c^T \phi(t), \tag{15}$$

where, $\phi(t)^T = [x_0(t), x_1(t), \ldots, x_m(t)]$. The coefficient vector c is obtained from

$$c^T = \left(\int_{a_0}^{b_0} f^*(t)\phi(t)^T dt \right) Q^{-1}, \qquad Q = \int_{a_0}^{b_0} \phi(t)\phi(t)^T dt. \tag{16}$$

Theorem 2.1. *([33]). Let Y be a finite-dimensional closed subspace of a Hilbert space G with basis $\{y_1, \ldots, y_n\}$. If $z \in G$ and $y_0 \in Y$ is its best approximation, then*

$$\|z - y_0\|_2^2 = \frac{\Gamma(z, y_1, \ldots, y_n)}{\Gamma(y_1, \ldots, y_n)},$$

where, $\Gamma(\cdot)$ is the Gram determinant

$$\Gamma(z, y_1, y_2, \cdots, y_n) = \begin{vmatrix} \langle z, z\rangle & \langle z, y_1\rangle & \cdots & \langle z, y_n\rangle \\ \langle y_1, z\rangle & \langle y_1, y_1\rangle & \cdots & \langle y_1, y_n\rangle \\ \vdots & \vdots & \cdots & \vdots \\ \langle y_n, z\rangle & \langle y_n, y_1\rangle & \cdots & \langle y_n, y_n\rangle \end{vmatrix}.$$

Using Theorem 2.1, the approximation error can be expressed explicitly.

Since $\{H_1(0,x), H_1(1,x), \ldots, H_1(M,x)\}$ is linearly independent, any function $\hat{f}(x) \in L^2[a,b]$ admits the approximation

$$\hat{f}(x) \approx \sum_{i=0}^{M} e_i H_1(i,x) = E^T \psi_1(x), \tag{17}$$

where, $\psi_1(x)^T = [H_1(0,x), \ldots, H_1(M,x)]$. The coefficient vector is given by:

$$E^T = \left(\int_a^b \hat{f}(x)\psi_1(x)^T w_1(x)dx \right) Q_x^{-1}, \qquad Q_x = \int_a^b \psi_1(x)\psi_1(x)^T w_1(x)dx, \tag{18}$$

where, $w_1(x)$ denotes an appropriate weighting function.

Similarly, a two-variable function $g(x,y)$ on $[a,b] \times [c,d]$ can be approximated as

$$g(x,y) \approx \psi_1^T(x)\, G\, \psi_2(y), \tag{19}$$

where, $\psi_2(y)^T = [H_2(0,y), \ldots, H_2(M,y)]$ and

$$G = Q_x^{-1} \left(\int_a^b \int_c^d g(x,y)\psi_1(x)\psi_2(y)^T w_1(x)w_2(y)\, dx\, dy \right) Q_y^{-1}, \tag{20}$$

with $Q_y = \int_c^d \psi_2(y)\psi_2(y)^T w_2(y)dy$.

3 Error analysis

In this subsection, we analyze the approximation error associated with the proposed scheme.

Let $\Pi_{n,m}$ denote the space of bivariate polynomials

$$\Pi_{n,m} = \left\{ p(x,y) = \sum_{i=0}^{n} \sum_{j=0}^{m} a_{ij} x^i y^j : \ a_{ij} \in \mathbb{R} \right\}.$$

Let $F = \{(x_i, y_j) : 0 \le i \le n, \ 0 \le j \le m\}$ be a set of distinct nodes with

$$a = x_0 < \cdots < x_n = b, \qquad c = y_0 < \cdots < y_m = d.$$

A polynomial $P^*(x,y)$ is called the two-dimensional interpolating polynomial of $f(x,y)$ if

$$P^*(x_i, y_j) = f(x_i, y_j), \qquad \forall (x_i, y_j) \in F.$$

The upper bound of the two-dimensional interpolation error depends on the interpolation method and the smoothness of the target function $f(x,y)$. The following theorem is applicable to interpolation polynomials derived from Newton's divided difference formulas or Lagrange functions.

Theorem 3.1. *([34]). Let $(x_i, y_j) \in F$ and consider the function $f(x,y)$ has continuous partial derivatives of orders $m+1$ and $n+1$ with respect to x and y, respectively, and the relevant mixed derivative of order $m+n+2$ exists, then for all $(x,y) \in [x_0, x_n] \times [y_0, y_m]$ there exist $\xi, \xi' \in (x_0, x_n)$, $\eta, \eta' \in (y_0, y_m)$ such that*

$$f(x,y) - P^*(x,y) = \frac{1}{(n+1)!} \frac{\partial^{n+1} f(\xi, y)}{\partial x^{n+1}} \prod_{i=0}^{n} (x - x_i)$$

$$+ \frac{1}{(m+1)!} \frac{\partial^{m+1} f(x,\eta)}{\partial y^{m+1}} \prod_{j=0}^{m} (y - y_j) - \frac{1}{(n+1)!(m+1)!} \frac{\partial^{n+m+2} f(\xi', \eta')}{\partial x^{n+1} \partial y^{m+1}} \prod_{i=0}^{n} (x - x_i) \prod_{j=0}^{m} (y - y_j),$$

which the polynomial $P^*(x,y)$ is the two-dimensional interpolating polynomial of function $f(x,y)$ with respect to points set F.

Theorem 3.2. *([34, 35]). Let $f \in C^{M+1}([a,b]\times[c,d])$ and let $P^*(x,y)$ be the interpolating polynomial of degree M. Then,*

$$|f(x,y)-P^*(x,y)| \le \frac{H_{M+1}}{((M+1)!)^2}\prod_{i=0}^{M}|x-x_i|\prod_{j=0}^{M}|y-y_j|,$$

where,

$$H_{M+1}=\max_{0\le k\le M+1}\left\|\frac{\partial^{M+1}f}{\partial x^k\partial y^{M+1-k}}\right\|_\infty.$$

Lemma 3.3. *Let $f(x,y)\in C^{M+1}([a,b]\times[c,d])$ satisfy homogeneous boundary conditions*

$$f(a,y)=f(b,y)=f(x,c)=f(x,d)=0.$$

Let $Y=\mathrm{Span}\{H_1(0,x),\dots,H_1(M,x),H_2(0,y),\dots,H_2(M,y)\}$ and let $y^*(x,y)$ be the best approximation of f from Y. Then,

$$\|f-y^*\|_2 \le \frac{H_{M+1}(b-a)^{\frac{2M+3}{2}}(d-c)^{\frac{2M+3}{2}}}{((M+1)!)^2}.$$

Proof. Let $P^*(x,y)$ denote the interpolating polynomial of $f(x,y)$ at grid points $\{(x_i,y_j)\}$. Since $P^*(x,y)\in Y$ and y^* is the best approximation, we have:

$$\|f-y^*\|_2 \le \|f-P^*\|_2 \le \sqrt{(b-a)(d-c)}\|f-P^*\|_\infty.$$

Applying Theorem 3.2 yields the result. ■

From Lemma 3.3, the approximation error decreases as M increases, implying convergence of the proposed method.

3.1 Convergence analysis

In this subsection, we establish the convergence behavior of the proposed approximation scheme and discuss its convergence rate.

Theorem 3.4 (Spectral convergence rate)**.** *Assume f is analytic on the closed domain $[a,b]\times[c,d]$ (i.e., f extends analytically to an open neighborhood in $\mathbb{C}^2$) and that the orthonormal bases $\{\phi_i\},\{\psi_j\}$ consist of orthogonal polynomials (e.g., Legendre, Chebyshev, or Gegenbauer). Then there exist constants $C>0$ and $\rho>1$, independent of M, such that*

$$\|f-y_M^*\|_2 \le C\rho^{-M}.$$

Proof. For analytic functions on $[-1,1]$, the expansion coefficients in orthogonal polynomials decay exponentially. More precisely (see [31, 32]), there exists $\rho>1$ such that

$$|\hat{f}_i| \le C_1\rho^{-i}, \quad \text{where } f(x)=\sum_{i=0}^{\infty}\hat{f}_iP_i(x),$$

with P_i the Legendre polynomials normalized in L^2. The constant ρ depends on the largest ellipse of analyticity in the complex plane.

For a bivariate analytic function $f(x, y)$ on $[-1, 1]^2$, its expansion

$$f(x, y) = \sum_{i=0}^{\infty} \sum_{j=0}^{\infty} \hat{f}_{ij} \phi_i(x) \psi_j(y),$$

has coefficients satisfying

$$|\hat{f}_{ij}| \leq C_2 \rho^{-i} \sigma^{-j},$$

with $\rho, \sigma > 1$. If the bases are of the same type and the domain symmetric, we take $\rho = \sigma$.

The truncated series

$$f_M(x, y) = \sum_{i=0}^{M} \sum_{j=0}^{M} \hat{f}_{ij} \phi_i(x) \psi_j(y),$$

lies in Y_M. Its error is bounded by

$$\|f - f_M\|_2^2 \leq \sum_{i=M+1}^{\infty} \sum_{j=0}^{\infty} |\hat{f}_{ij}|^2 + \sum_{i=0}^{M} \sum_{j=M+1}^{\infty} |\hat{f}_{ij}|^2.$$

Using the exponential bound on $|\hat{f}_{ij}|$, each term is $O(\rho^{-2(M+1)})$. Hence

$$\|f - f_M\|_2 \leq C_3 \rho^{-(M+1)}.$$

Since y_M^* is the *best* approximation,

$$\|f - y_M^*\|_2 \leq \|f - f_M\|_2 \leq C \rho^{-M},$$

by redefining constants. ■

If f satisfies homogeneous Dirichlet boundary conditions ($f = 0$ on the boundary of the rectangle), the bases $\{\phi_i\}$ and $\{\psi_j\}$ should be chosen to satisfy the same boundary conditions (e.g., $\phi_i(a) = \phi_i(b) = 0$). In that case, the above results hold unchanged because the completeness of such bases in the Sobolev space H_0^1 implies completeness in L^2. The exponential convergence rate remains valid if f is analytic and vanishes on the boundary.

Therefore, increasing M leads to a rapid (exponential) reduction of the approximation error, which explains the high accuracy observed in the numerical experiments.

Preservation of spectral convergence

A crucial theoretical consideration is whether the transition from a strictly orthogonal Gegenbauer basis to the semi-orthogonal basis $\{H_1(k, x)\}$ compromises the spectral convergence rate characteristic of global projection methods. We establish here that the spectral convergence behavior remains entirely intact.

Let $u(x)$ be a sufficiently smooth function defined on $[0, L_1]$. In a standard Gegenbauer pseudospectral or Galerkin expansion, the approximation error $e_N = \|u - u_N\|$ is governed by the regularity of $u(x)$. If $u(x) \in C^{\infty}([0, L_1])$, the expansion coefficients decay exponentially, i.e., $|\hat{u}_k| \leq M e^{-\sigma k}$ for positive constants M and σ.

Because each semi-orthogonal basis function $H_1(k, x)$ is constructed as a finite, localized linear combination of exactly three consecutive Gegenbauer polynomials:

$$H_1(k, x) = C_{k+2}^{\lambda}(\xi) + \alpha C_{k+1}^{\lambda}(\xi) + \beta C_k^{\lambda}(\xi), \tag{21}$$

the transformation matrix T mapping the standard Gegenbauer coefficient vector $\hat{\mathbf{u}}$ to the semi-orthogonal coefficient vector $\mathbf{c}$ (such that $\hat{\mathbf{u}} = T\mathbf{c}$) is a banded upper-triangular matrix with a bounded condition number. Consequently, the coefficients c_k inherit the exact same asymptotic decay rate as the orthogonal coefficients:

$$|c_k| \sim \mathcal{O}\left(e^{-\sigma k}\right), \quad \text{as } k \to \infty. \tag{22}$$

Thus, the semi-orthogonal expansion retains the capability to capture the solution with exponential accuracy ("spectral accuracy"), ensuring that the geometric reduction in computational complexity ($\mathcal{O}(N)$ matrix operations) does not incur any mathematical penalty regarding convergence velocity.

4 Methodology

To homogenize the boundary conditions of the main problem (1), we introduce the decomposition

$$u(x, y) = v(x, y) + w(x, y),$$

where $w(x, y)$ is the interpolation function constructed in Subsection 2.1. Substituting this decomposition into Equation (1) yields the following equivalent homogenized Helmholtz equation:

$$\nabla^2 v + f(x, y)v(x, y) = g_1(x, y), \tag{23}$$

where,

$$g_1(x, y) = g(x, y) - \left(\nabla^2 w(x, y) + f(x, y)w(x, y)\right).$$

The corresponding homogeneous Dirichlet boundary conditions become

$$v(a, y) = 0, \quad v(b, y) = 0, \quad c < y < d, \tag{24}$$

and

$$v(x, c) = 0, \quad v(x, d) = 0, \quad a < x < b. \tag{25}$$

Based on the approximation framework developed in Subsection 2.4, the unknown function $v(x, y)$ is approximated as

$$v(x, y) = \psi_1^T(x)\, C\, \psi_2(y),$$

where $C \in \mathbb{R}^{(M+1)\times(M+1)}$ is the matrix of unknown coefficients, and it is determined such that the approximation satisfies Equation (23) together with the boundary conditions (24)–(25).

Due to the construction of the homogenizing Gegenbauer basis functions $H_1(k, x)$ and $H_2(k, y)$ in Equations (13) and (14), the boundary conditions are automatically satisfied by the approximation space.

Next, we define the residual function as:

$$\begin{aligned} R(x, y) &= \nabla^2 v + f(x, y)v(x, y) - g_1(x, y) \\ &= \psi_1''(x)^T C\psi_2(y) + \psi_1(x)^T C\psi_2''(y) + f(x, y)v(x, y) - g_1(x, y), \end{aligned}$$

where, ψ_1'' and ψ_2'' denote second derivatives with respect to x and y, respectively.

To determine the coefficient matrix C, the Galerkin method is employed. This leads to the following system of algebraic equations:

$$\int_a^b \int_c^d R(x, y)\, H_1(i, x)\, H_2(j, y)\, w_1(x) w_2(y)\, dx\, dy = 0, \quad i, j = 0, 1, \ldots, M.$$

The resulting nonlinear algebraic system is solved using symbolic or numerical computation software (e.g., MATHEMATICA). The proposed scheme is straightforward in implementation while exhibiting high numerical accuracy and stability, as demonstrated in the subsequent section.

5 Numerical results

In this section, several benchmark problems are presented to evaluate the performance of the proposed method. The numerical experiments are designed to assess accuracy, convergence behavior, stability under perturbations, and computational efficiency. To assess the method's performance, the Root Mean Square Error (RMSE) is calculated

$$RMSE = \sqrt{\frac{1}{(d-c)(b-a)} \int_c^d \int_a^b \big(u_M(x,y) - u^*(x,y)\big)^2 w_1(x) w_2(y)\, dxdy}, \tag{26}$$

where $u_M(x,y)$ and $u^*(x,y)$ refer to the approximate solution calculated using a polynomial of order M and the exact solution, respectively. RMSE quantifies the average deviation of $u_M(x,y)$ from $u^*(x,y)$ over the entire domain in an L^2-sense. The RMSE values for each example are displayed in Table 1. The computational efficiency of the proposed scheme is demonstrated by presenting the whole CPU time required to compute the approximate solution in Table 1. As expected from the fast convergence rate, the error decays fast with respect to the degrees of freedom. This favorable behavior demonstrates that high accuracy can be achieved with relatively low CPU times compared to low-order methods. In the subsequent calculations, the value of $\lambda = \frac{1}{2}$ is taken into account.

Table 1: Numerical results including RMSE and CPU time (seconds) for different examples.

	Ex. 5.1 ($M=3$)	Ex. 5.2 ($M=4$)	Ex. 5.3 ($M=3$)	Ex. 5.4 ($M=2$)	Ex. 5.5 ($M=3$)	Ex. 5.6 ($M=3$, a=1)	Ex. 5.6 ($M=3$, a=2)
RMSE	8.50×10^{-5}	6.23×10^{-6}	6.21×10^{-4}	0	2.10×10^{-4}	1.43×10^{-6}	4.69×10^{-6}
CPU (s)	4.51	4.90	4.26	3.00	4.71	4.26	4.31

Example 5.1. Consider the Helmholtz equation in the Cartesian coordinate system [25]:

$$\begin{aligned} &\nabla^2 u(x,y) + \lambda_0^2 u(x,y) = -\sin(x)\sin\left(\frac{y}{2}\right), \\ &u(0,y) = u(\pi,y) = u(x,0) = 0, \quad u(x,\pi) = \sin(x), \end{aligned} \tag{27}$$

where, the exact solution is $u^*(x,y) = \sin(x)\sin(\lambda_0 y)$ with $\lambda_0 = 1/2$ on the domain $\Omega = [0,\pi]\times[0,\pi]$. Applying Equation (10) to the boundary conditions in (27) yields

$$w(x,y) = \frac{y\sin(x)}{\pi}.$$

By executing the numerical method detailed in Section 4, the solution is decomposed as $u(x,y) = v(x,y) + w(x,y)$.

The error function, defined as $u_M(x,y) - u^*(x,y)$, is illustrated in the left panel of Figure 1, demonstrating the satisfactory accuracy of the proposed method. The right panel displays the corresponding contour plot, highlighting the spatial distribution of the approximation error. Furthermore, the RMSE values presented in Table 1 support these observations.

To evaluate the stability of the method, we analyze the following system for perturbation parameters $\epsilon = 10^{-2}$ and 10^{-4}:

$$\begin{aligned} &\nabla^2 u(x,y) + \lambda_0^2 u(x,y) = -\sin(x)\sin\left(\frac{y}{2}\right), \\ &u(0,y) = u(\pi,y) = u(x,0) = 0, \quad u(x,\pi) = (1-\epsilon)\sin(x). \end{aligned} \tag{28}$$

Applying Equation (10) to the perturbed conditions in (28) results in $w(x,y) = \frac{y(1-\epsilon)\sin(x)}{\pi}$. This modification facilitates an investigation into how minor perturbations in the boundary conditions influence the approximate solution. The RMSE values summarized in Table 2 indicate that small variations in the boundary lead to negligible changes in the approximation, serving as a robust indicator of the stability of the outlined numerical scheme.

Table 2: RMSE values for the perturbed equation in Example 5.1.

ϵ	10^{-2}	10^{-4}
RMSE	0.00276449	0.000498579

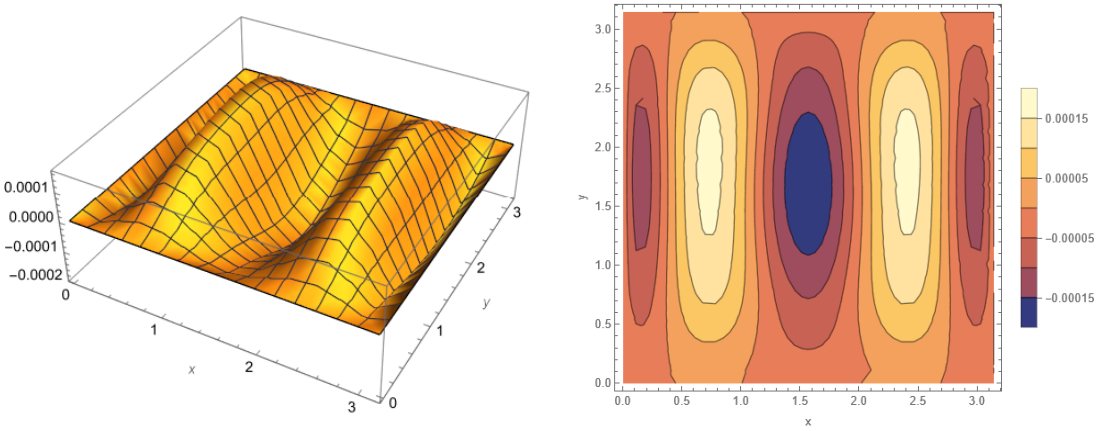


Figure 1: (Left) Error function and (right) contour plot of the error function for Example 5.1.

Example 5.2. We consider the Helmholtz equation [25]

$$\begin{aligned} &\nabla^2 u(x,y) + \lambda_0^2 u(x,y) = \left(\frac{1}{4} - 2\pi^2\right)\sin(\pi x)\sin(\pi y), \quad (x,y) \in [0,1]\times[0,1], \\ &u(0,y) = u(1,y) = u(x,0) = u(x,1) = 0, \end{aligned} \tag{29}$$

where, $\lambda_0 = \frac{1}{2}$. The exact solution is $u^*(x,y) = \sin(\pi x)\sin(\pi y)$.

Implementing the boundary conditions Equation (10) to Equation (29) gives $w(x,y) = 0$. Therefore, following the framework described in Section 4, the function $u(x,y)$ simplifies to $v(x,y)$. The RMSE results presented in Table 1 confirm that the method attains high accuracy. The numerical results reported in Table 1 demonstrate that the proposed approximation scheme achieves high precision for the Helmholtz problem. This behavior is consistent with the theoretical convergence results established in Theorem 3.4.

Unlike the finite-difference framework, where boundary conditions are enforced pointwise on a discrete grid and high accuracy is achieved through iterative refinement (block-AGE iteration) combined with a sixth-order compact stencil, the present approach embeds the boundary data analytically into a single closed-form interpolation function, after which the homogenized problem is solved by a global spectral expansion with no grid refinement required.

Example 5.3. Suppose the Poisson equation [25]

$$\begin{aligned} &\nabla^2 u(x,y) + \lambda_0^2 u(x,y) = (4-\pi^2)\exp(2x)\sin(\pi y), \quad (x,y) \in [0,1]\times[0,1], \\ &u(0,y) = \sin(\pi y), \quad u(1,y) = \exp(2)\sin(\pi y), \quad u(x,0) = 0, \quad u(x,1) = 0. \end{aligned} \tag{30}$$

Let $\lambda_0 = 0$. In this case, the exact solution is given by $u^*(x,y) = \exp(2x)\sin(\pi y)$. By applying Equation (10) under the boundary conditions specified in (30), the corresponding interpolation function is obtained as:

$$w(x,y) = x\big(\exp(2)\sin(\pi y) - \sin(\pi y)\big) + \sin(\pi y).$$

Following the methodology outlined in Section 4, the solution is represented in the form $u(x,y) = v(x,y) + w(x,y)$.

The resulting RMSE values, reported in Table 1, indicate a high level of agreement between the numerical and exact solutions. Notably, this level of accuracy is achieved with a relatively low polynomial order ($M = 3$), highlighting the efficiency and strong approximation capability of the method in comparison with the method presented in [25].

Example 5.4. Consider the Poisson equation [24]

$$\begin{aligned} &u_{xx} + u_{yy} = xe^y, \quad (x,y) \in [0,2]\times[0,1], \\ &u(0,y) = 0, \quad u(2,y) = 2e^y, \quad u(x,0) = x, \quad u(x,1) = xe. \end{aligned} \tag{31}$$

This problem arises in various physical applications, such as steady-state heat conduction and electrostatic potential modeling, where the source term exhibits an exponential spatial variation. The exact solution is given by $u^*(x,y) = xe^y$, which allows for a direct and reliable assessment of numerical accuracy.

Substituting the boundary conditions (31) into Equation (10) yields the interpolation function $w(x,y) = xe^y$. According to the methodology presented in Section 4, the solution can be expressed as $u(x,y) = v(x,y) + w(x,y)$.

The accuracy of the proposed method is evaluated through the error function $u_M(x,y) - u^*(x,y)$. As reported in Table 1, the RMSE value is zero (within machine precision), indicating that the numerical solution coincides with the exact solution. This result demonstrates the capability of the method to recover the exact solution when it belongs to the approximation space, highlighting its high-order accuracy and fast convergence behavior.

To further examine the stability and robustness of the method, a perturbed version of the problem is considered:

$$\begin{aligned} &u_{xx} + u_{yy} = (1-\epsilon)xe^y, \quad (x,y) \in [0,2]\times[0,1], \\ &u(0,y) = 0, \quad u(2,y) = 2e^y, \quad u(x,0) = x, \quad u(x,1) = xe, \end{aligned}$$

for $\epsilon = 10^{-2}, 10^{-4}, 10^{-6}$.

This perturbation enables the investigation of how small variations in the source term affect the numerical solution. Using the same interpolation function $w(x,y) = xe^y$, the main equation is transformed into the homogenized form

$$v_{xx} + v_{yy} + \epsilon\, xe^y = 0, \qquad v(0,y) = v(2,y) = v(x,0) = v(x,1) = 0.$$

The RMSE values for the perturbed problem, presented in Table 3, indicate that the numerical error decreases proportionally with ϵ. This behavior confirms that the proposed method is stable with respect to perturbations in the source term and exhibits a well-conditioned numerical structure.

Table 3: RMSE values for the perturbed equation in Example 5.4 under varying ϵ.

ϵ	10^{-2}	10^{-4}	10^{-6}
RMSE	6.1536×10^{-3}	6.1536×10^{-5}	6.1536×10^{-7}

Overall, this example demonstrates not only the high accuracy of the proposed method but also its strong stability properties and its ability to handle problems with exponentially varying source terms effectively.

Example 5.5. Consider the Helmholtz equation [24, 36]

$$\begin{aligned} &\nabla^2 u(x,y) + 5u(x,y) = 0, \quad (x,y) \in [0,1] \times [0,1], \\ &u(0,y) = 0, \quad u(1,y) = \sin(3)\sinh(2y), \quad u(x,0) = 0, \quad u(x,1) = \sin(3x)\sinh(2), \end{aligned} \tag{32}$$

with the exact solution given by $u^*(x,y) = \sin(3x)\sinh(2y)$.

Application of Equation (10) under the boundary conditions (32) yields the interpolation function

$$w(x,y) = y\big(-x\sin(3)\sinh(2) + \sin(3x)\sinh(2)\big) + x\sin(3)\sinh(2y),$$

thus $u(x,y) = v(x,y) + w(x,y)$.

The accuracy of the proposed method is assessed using the RMSE metric reported in Table 1. Table 1 demonstrates that the proposed scheme yields accurate numerical results with minimal deviation from the exact solution, thereby confirming the effectiveness and reliability of the method for this class of Helmholtz problems.

Example 5.6. Consider the Helmholtz equation [24, 37]

$$\begin{aligned} &\nabla^2 u(x,y) + a^2 u(x,y) = (a^2-5)\sin(x)\sin(2y), \quad (x,y) \in [0,1] \times [0,1], \\ &u(0,y) = 0, \quad u(1,y) = \sin(1)\sin(2y), \quad u(x,0) = 0, \quad u(x,1) = \sin(x)\sin(2), \end{aligned} \tag{33}$$

whose exact solution is given by $u^*(x,y) = \sin(x)\sin(2y)$ for $a = 1, 2$ on the domain $[0,1]\times[0,1]$.

By incorporating the boundary conditions (33) into Equation (10), the interpolation function is obtained as:

$$w(x,y) = y\big(-x\sin(1)\sin(2) + \sin(2)\sin(x)\big) + x\sin(1)\sin(2y).$$

Accordingly, the solution is represented in the form $u(x,y) = v(x,y) + w(x,y)$, as described in Section 4.

The performance of the proposed method is illustrated in Figures 2 and 3. The left plot depicts the error distribution $u_M(x,y) - u^*(x,y)$, while the right plot illustrates the spatial dispersion of the error through its contour representation. The results demonstrate that the error remains uniformly small across the computational domain. This observation is further supported by the low RMSE value reported in Table 1, confirming the high accuracy of the method.

Example 5.7. In the preceding examples, the exact solutions were separable and the coefficient function $f(x,y)$ was constant. However, many practical problems involve non-separable

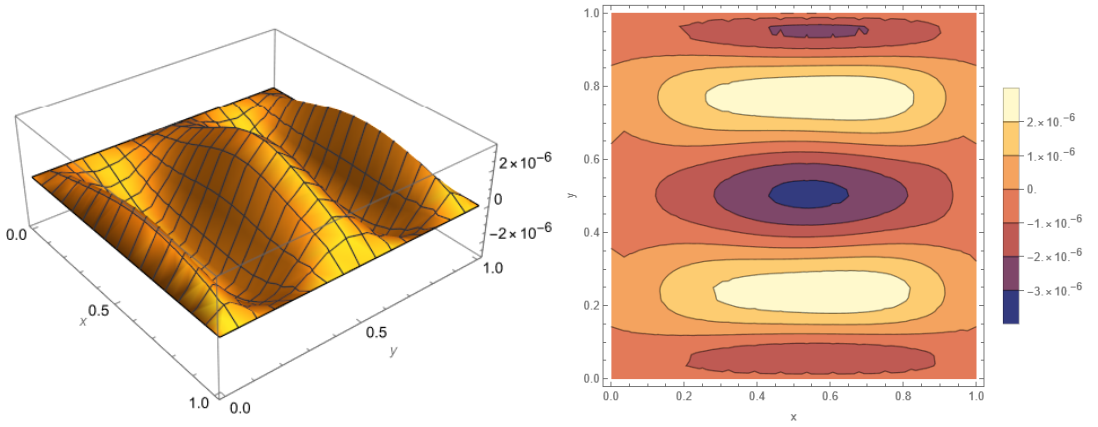


Figure 2: (Left) Error function and (right) contour plot of the error function with $a = 1$ for Example 5.6.

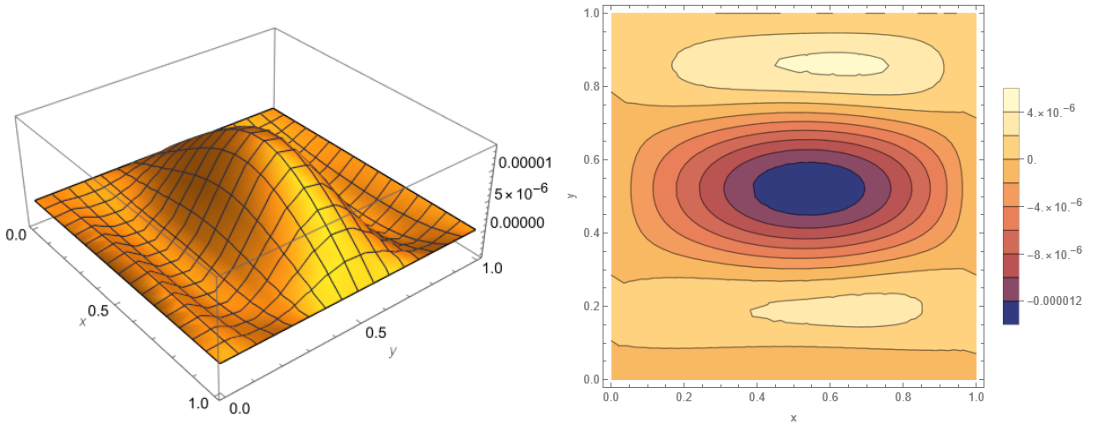


Figure 3: (Left) Error function and (right) contour plot of the error function with $a = 2$ for Example 5.6.

solutions and variable coefficients. To demonstrate the robustness and general applicability of the proposed method, we consider the following Helmholtz equation with an inseparable exact solution:

$$\nabla^2 u(x,y) + (x-1)u(x,y) = 2x^2 + 6y + 2y^2 + (-1+x)(2+6x+x^2y^2+y^3),$$
$$u(0,y) = y^3 + 2, \quad u(2,y) = 4y^2 + y^3 + 14, \tag{34}$$
$$u(x,0) = 6x + 2, \quad u(x,2) = 4x^2 + 6x + 10, \tag{35}$$

whose exact solution is given by $u^*(x,y) = x^2y^2 + 6x + y^3 + 2$ on the domain $[0,2] \times [0,2]$. It is evident that this solution is non-separable, providing a more challenging test for the numerical scheme.

Applying Equation (10) together with the boundary conditions (34) and (35) yields the interpolation function

$$w(x,y) = \frac{1}{2}(4x^2 - 8x)y + \frac{1}{2}x(4y^2 + 12) + y^3 + 2.$$

Following the methodology outlined in Section 4, the solution is represented as $u(x,y) = v(x,y) + w(x,y)$.

The numerical performance of the method is illustrated in Figure 4, which depicts the error distribution $u_M(x,y) - u^*(x,y)$. The results show that the error remains negligibly small across the entire domain. For $M = 3$, the RMSE is 7.77026×10^{-16}, indicating that the numerical solution is essentially indistinguishable from the exact solution within machine precision.

These findings highlight the capability of the proposed method to accurately approximate solutions of Helmholtz problems with variable coefficients and inseparable exact solutions, demonstrating both its flexibility and high computational efficiency.

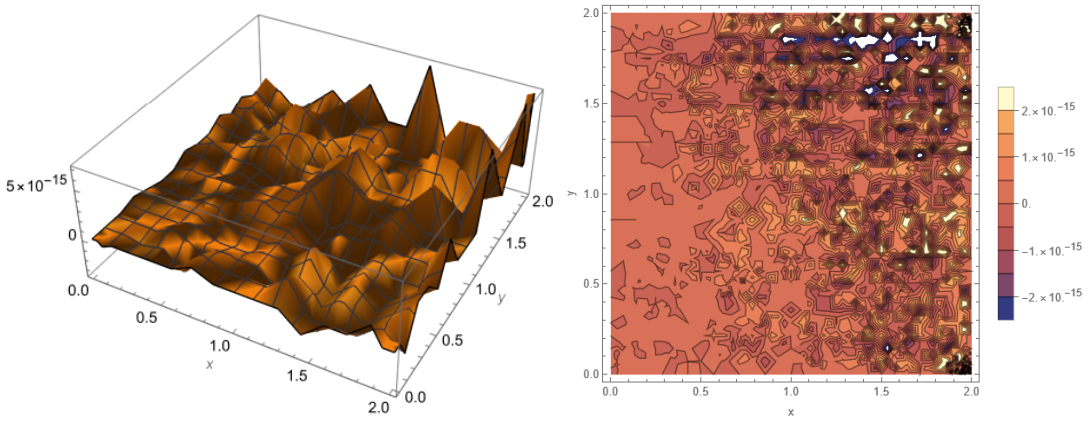


Figure 4: (Left) Error function and (right) contour plot of the error function for Example 5.7.

Example 5.8. Consider the well-known two-dimensional Poisson equation [38–42]:

$$\nabla^2 u = 1, \qquad (x,y) \in (0,1) \times (0,1),$$

subject to the homogeneous Dirichlet boundary conditions

$$u = 0 \text{ on } \partial\Omega.$$

The analytical solution is given by the double Fourier sine series:

$$u(x,y) = -\frac{16}{\pi^4} \sum_{m=1}^{\infty} \sum_{n=1}^{\infty} \frac{\sin\big((2m-1)\pi x\big) \sin\big((2n-1)\pi y\big)}{(2m-1)(2n-1)\left[(2m-1)^2 + (2n-1)^2\right]}.$$

Due to the constant source term ($g(x,y) = 1$) and the unit square domain with homogeneous Dirichlet boundary conditions, this serves as a classic benchmark problem often referred to as the torsion problem (or a uniform load on a square plate).

The proposed method is applied here with $M = 3$ and $M = 4$, and the corresponding numerical results are presented in Figure 5. As the figure shows, the method yields a continuous solution with high accuracy together with a fast convergence rate.

As shown in Table 4, the approaches by Mebrate and Koya [41]-namely the finite difference and finite element methods for the Poisson equation- are restricted to evaluating approximate solutions at discrete grid points. In contrast, Figure 5 establishes a highly accurate approximation over the entire rectangular domain, yielding an error magnitude bounded by 10^{-5}. While our scheme delivers the approximate solution within only a single iteration, the method

referenced in Table 4 demands iterative refinement (frequently up to 15 iterations) to enhance precision. This significant difference in computational cost is corroborated by the findings reported in their paper.

Also, this problem was previously investigated by Kahlaf et al. [39] using three distinct approaches: the five-point finite difference method, the nine-point finite difference method, and the finite element method for the Helmholtz equation. The corresponding numerical results are summarized in Table 5. As shown in Table 5, the accuracy of the three existing methods is limited to 10^{-2}. In contrast, Figure 5 highlights that our method achieves a significantly higher accuracy, dropping below 10^{-4}. Compared to the five-point finite difference, nine-point finite difference, and finite element methods presented in [39], our proposed approach offers a remarkably straightforward implementation. Furthermore, while the methods in [39] yield solutions exclusively at discrete nodal points, our method provides a smooth approximate solution over the entire domain $\forall(x, y) \in [0, 1] \times [0, 1]$. This comparative data validates the enhanced computational efficiency of the proposed method when evaluated under identical problem constraints.

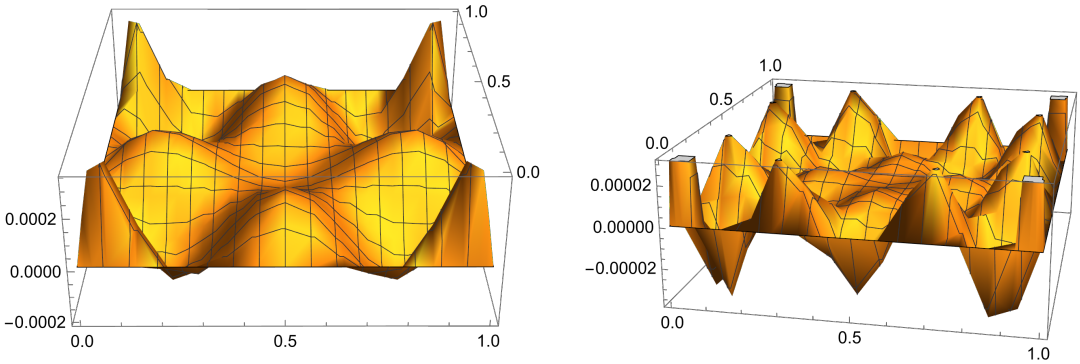


Figure 5: The error function obtained with $M = 3$ (left) and $M = 4$ (right) for Example 5.8.

Table 4: Comparison of numerical solutions $u(x, y)$ at specific nodal points for Example 5.8.

Nodes (x, y)	FDM [41]	FEM [41]	Proposed Method
$v_7 = (0.25, 0.25)$	-0.0430	-0.0391	-0.0452937
$v_8 = (0.25, 0.50)$	-0.0547	-0.0573	-0.0573296
$v_9 = (0.25, 0.75)$	-0.0430	-0.0391	-0.0452937
$v_{12} = (0.50, 0.25)$	-0.0547	-0.0573	-0.0573296
$v_{13} = (0.50, 0.50)$	-0.0703	-0.0677	-0.0736717
$v_{14} = (0.50, 0.75)$	-0.0547	-0.0573	-0.0573296
$v_{17} = (0.75, 0.25)$	-0.0430	-0.0391	-0.0452937
$v_{18} = (0.75, 0.50)$	-0.0547	-0.0573	-0.0573296
$v_{19} = (0.75, 0.75)$	-0.0430	-0.0391	-0.0452937

6 Conclusion

This research focused on developing an innovative approach for solving the two-dimensional Helmholtz problem, based on a generalized two-dimensional interpolation function and a new

Table 5: Numerical results obtained using the three baseline methods from [39] for Example 5.8.

Nodes (x, y)	Finite Difference Method (FDM)		Finite Element Method (FEM)
	Five-Point	Nine-Point	
$v_7 = (0.25, 0.25)$	-0.0422	-0.0454	-0.0391
$v_8 = (0.25, 0.50)$	-0.0539	-0.0574	-0.0573
$v_9 = (0.25, 0.75)$	-0.0426	-0.0454	-0.0391
$v_{12} = (0.50, 0.25)$	-0.0539	-0.0574	-0.0573
$v_{13} = (0.50, 0.50)$	-0.0695	-0.0737	-0.0677
$v_{14} = (0.50, 0.75)$	-0.0543	-0.0574	-0.0573
$v_{17} = (0.75, 0.25)$	-0.0426	-0.0454	-0.0391
$v_{18} = (0.75, 0.50)$	-0.0543	-0.0574	-0.0573
$v_{19} = (0.75, 0.75)$	-0.0428	-0.0454	-0.0391

class of homogenizing Gegenbauer polynomials (HGPs). The essential conditions required for the formulation of the proposed interpolation framework were systematically derived and discussed, and it was shown that the resulting HGP basis is semi-orthogonal, with a Gram matrix that remains banded (at most pentadiagonal) regardless of the approximation order, thereby preserving the computational efficiency characteristic of spectral methods while enforcing homogeneous boundary conditions exactly. Using this basis, the original nonhomogeneous Helmholtz problem was transformed into an equivalent homogeneous one and solved via a Galerkin projection, reducing the problem to a system of algebraic equations. It was further shown that, although the interpolation problem does not generally admit a unique representation, the proposed construction is capable of recovering the exact solution within the admissible functional space. To analyze the convergence behavior of the approximation scheme, an explicit upper bound for the function approximation error was established, together with a spectral (exponential) convergence rate for analytic solutions; this provides a theoretical justification for the numerical performance observed. The numerical experiments, spanning eight benchmark Helmholtz and Poisson problems with separable and non-separable exact solutions, confirm that the proposed method achieves RMSE values as low as machine precision (e.g., 7.77×10^{-16} in Example 7) at low polynomial degree, with CPU times under 5 seconds for all reported cases. The method was also shown to remain stable under small perturbations of the boundary data and source term. Despite its relatively simple structure, the method exhibits precision and robustness that compare favorably with existing finite difference, finite element, and spectral element approaches reported in the literature.

Future research directions: Several promising extensions of the present work can be considered.

- **Higher-dimensional problems.** A natural continuation is the generalization of the proposed framework to three-dimensional Helmholtz and Poisson-type equations, where the construction of homogenizing interpolation functions and the corresponding tensor-product HGP bases becomes considerably more intricate.

- **Fractional partial differential equations.** Extending the method to fractional PDEs is an important direction. Developing homogenizing interpolation and spectral representations for fractional derivatives (e.g., Caputo or Riesz-type operators) would broaden the applicability of the approach to anomalous diffusion, viscoelasticity, and other nonlocal phenomena.

- **Nonlinear and time-dependent problems.** Adapting the method to evolutionary Helmholtz-type models and nonlinear reaction–diffusion systems is another valuable direction, where stability and convergence properties would require further investigation.

Author contributions. It is hereby declared that all authors contributed equally to the conception, development, and preparation of the manuscript.

Conflicts of Interest. The authors declare that they have no conflicts of interest regarding the publication of this article.

References

[1] L. L. Thompson, A review of finite-element methods for time-harmonic acoustics, *J. Acoust. Soc. Am.* **119** (2006) 1315–1330, https://doi.org/10.1121/1.2164987.

[2] A. De La Bourdonnaye, Some formulations coupling finite element and integral equation methods for Helmholtz equation and electromagnetism, *Numer. Math.* **69** (1995) 257–268, https://doi.org/10.1007/s002110050091.

[3] J.-H. Li, X.-Y. Hu, S.-H. Zeng, J.-G. Lu, G.-P. Huo, B. Han and R.-H. Peng, Three-dimensional forward calculation for loop source transient electromagnetic method based on electric field Helmholtz equation, *Chin. J. Geophys.* **56** (2013) 4256–4267.

[4] B. R. McLeod, A. A. Pilla and M. W. Sampsel, Electromagnetic fields induced by Helmholtz aiding coils inside saline-filled boundaries, *Bioelectromagnetics* **4** (1983) 357–370, https://doi.org/10.1002/bem.2250040407.

[5] D. M. Pozar, *Microwave Engineering*, Fourth ed., John Wiley & Sons, Inc, 2012.

[6] N. H. Tuan, V. A. Khoa, M. N. Minh and T. Tran, Reconstruction of the electric field of the Helmholtz equation in three dimensions, *J. Comput. Appl. Math.* **309** (2017) 56–78.

[7] I. Baydoun, D. Baresch, R. Pierrat and A. Derode, Radiative transfer of acoustic waves in continuous complex media: Beyond the Helmholtz equation, *Phys. Rev. E* **94** (2016) #053005.

[8] W. Tobocman, Calculation of acoustic wave scattering by means of the Helmholtz integral equation. II, *J. Acoust. Soc. Am.* **76** (1984) 1549–1554, https://doi.org/10.1121/1.391465.

[9] S.-A. Yang, Acoustic scattering by a hard or soft body across a wide frequency range by the Helmholtz integral equation method, *J. Acoust. Soc. Am.* **102** (1997) 2511–2520, https://doi.org/10.1121/1.420305.

[10] D. J. Griffiths and D. F. Schroeter, *Introduction to Quantum Mechanics*, Cambridge University Press, 2018.

[11] P. Amore, Solving the Helmholtz equation for membranes of arbitrary shape: numerical results, *J. Phys. A: Math. Theor.* **41** (2008) #265206, https://doi.org/ 10.1088/1751-8113/41/26/265206.

[12] S. Yu. Reutskiy, Vibration analysis of arbitrarily shaped membranes, *Comput. Model. Eng. Sci.* **51** (2009) 115–142, https://doi.org/10.3970/cmes.2009.051.115.

[13] B. Borden, Mathematical problems in radar inverse scattering, *Inverse Problems.* **18** (2001) R1–R28, https://doi.org/10.1088/0266-5611/18/1/201.

[14] W. S. Hall and X. Q. Mao, A boundary element investigation of irregular frequencies in electromagnetic scattering, *Eng. Anal. Bound. Elem.* **16** (1995) 245–252, https://doi.org/10.1016/0955-7997(95)00068-2.

[15] J. D. Anderson Jr., *Fundamentals of Aerodynamics*, McGraw-Hill, New York, 1991.

[16] S. A. Khan, Wavelength-dependent modifications in Helmholtz Optics, *Int. J. Theor. Phys.* **44** (2005) 95–125, https://doi.org/10.1007/s10773-005-1488-0.

[17] E. Hecht, *Optik*, Walter de Gruyter GmbH & Co KG, 2023.

[18] L. F. Canino, J. J. Ottusch, M. A. Stalzer, J. L. Visher and S. M. Wandzura, Numerical solution of the Helmholtz equation in 2D and 3D using a high-order Nyström discretization, *J. Comput. Phys.* **146** (1998) 627–663.

[19] G. Bao, G. W. Wei and S. Zhao, Numerical solution of the Helmholtz equation with high wavenumbers, *Internat. J. Numer. Methods Engrg.* **59** (2004) 389–408, https://doi.org/10.1002/nme.883.

[20] M. M. Gupta, J. Kouatchou and J. Zhang, Comparison of second-and fourth-order discretizations for multigrid Poisson solvers, *J. Comput. Phys.* **132** (1997) 226–232, https://doi.org/10.1006/jcph.1996.5466.

[21] D. Veerababu and P. K. Ghosh, Solving 2-D Helmholtz equation in the rectangular, circular, and elliptical domains using neural networks, *J. Sound Vib.* **607** (2025) #119022, https://doi.org/10.1016/j.jsv.2025.119022.

[22] A. Kaya and M. A. Freitag, Conditioning analysis for discrete Helmholtz problems, *Comput. Math. Appl.* **118** (2022) 171–182, https://doi.org/10.1016/j.camwa.2022.05.016.

[23] O. Z. Mehdizadeh and M. Paraschivoiu, Investigation of a two-dimensional spectral element method for Helmholtz's equation, *J. Comput. Phys.* **189** (2003) 111–129, https://doi.org/10.1016/S0021-9991(03)00204-3.

[24] M. Dehghan, M. Nourian and M. B. Menhaj, Numerical solution of Helmholtz equation by the modified Hopfield finite difference techniques, *Numer. Methods Partial Differential Equations* **25** (2009) 637–656, https://doi.org/10.1002/num.20366.

[25] R. K. Mohanty, Sixth order compact multi-phase block-AGE iteration methods for computing 2D Helmholtz equation, *MethodsX.* **12** (2024) #102633, https://doi.org/10.1016/j.mex.2024.102633.

[26] D. A. Juraev, P. Agarwal, E. E. Elsayed and N. Targyn, Applications of the Helmholtz equation, *Adv. Eng. Days* **8** (2023) 28–30.

[27] A. Szabo and N. S. Ostlund, *Modern Quantum Chemistry: Introduction to Advanced Electronic Structure Theory*, Courier Corporation, 1996.

[28] J. M. Thijssen, *Computational Physics*, 2nd ed., Cambridge University Press, Cambridge, 2007.

[29] G. Szegö, *Orthogonal Polynomials*, American Mathematical Society Colloquium Publications, Vol. 23, American Mathematical Society, Providence, RI, 1939.

[30] J. P. Boyd, *Chebyshev and Fourier Spectral Methods*, 2nd ed., Dover Publications, Mineola, NY, 2000.

[31] J. Shen, T. Tang and L.-L. Wang, *Spectral Methods: Algorithms, Analysis and Applications*, Springer, Berlin, 2011.

[32] C. Canuto, M. Y. Hussaini, A. Quarteroni and T. A. Zang, *Spectral Methods: Fundamentals in Single Domains*, Springer, Berlin, 2006.

[33] E. Kreyszig, *Introductory Functional Analysis with Applications*, John Wiley & Sons, 1991.

[34] E. Isaacson and H. B. Keller, *Analysis of Numerical Methods*, Courier Corporation, 2012.

[35] J. Stoer, R. Bulirsch, R. Bartels, W. Gautschi and C. Witzgall, *Introduction to Numerical Analysis*, Springer, New York, 1980.

[36] S. M. El-Sayed and D. Kaya, Comparing numerical methods for Helmholtz equation model problem, *Appl. Math. Comput.* **150** (2004) 763–773, https://doi.org/10.1016/S0096-3003(03)00305-9.

[37] I. Singer and E. Turkel, High-order finite difference methods for the Helmholtz equation, *Comput. Methods Appl. Mech. Engrg.* **163** (1998) 343–358, https://doi.org/10.1016/S0045-7825(98)00023-1.

[38] H. C. Elman, D. J. Silvester and A. J. Wathen, *Finite Elements and Fast Iterative Solvers: with Applications in Incompressible Fluid Dynamics*, 2nd ed., Oxford University Press, Oxford, 2014.

[39] S. J. Kahlaf and A. A. Mhassin, Numerical solution of a two-dimensional Helmholtz equation with Dirichlet boundary conditions, *J. Interdiscip. Math.* **24** (2021) 971–982, https://doi.org/10.1080/09720502.2021.1885815.

[40] R. Haberman, *Applied Partial Differential Equations with Fourier Series and Boundary Value Problems*, 5th ed., Pearson, Boston, 2012.

[41] B. Mebrate and P. R. Koya, Numerical solution of a two dimensional poisson equation with dirichlet boundary conditions, *Am. J. Appl. Math.* **3** (2015) 297–304, https://doi.org/10.11648/j.ajam.20150306.19.

[42] S. Timoshenko and J. N. Goodier, *Theory of Elasticity*, 3rd ed., McGraw-Hill, New York, 1970.